doi: 10.18720/MCE.78.2

The behavior of concentric brace with bounded fuse

Поведение концентрических раскосов с встроенным предохранителем по сжимающей нагрузке

M.A. Kafi,
A. Kachooee,
Semnan University, Semnan, Iran

PhD, доцент М.А. Кафя,
PhD А. Качуй,
Университет Семнан, г. Семнан, Иран

Key words: local fuse; concentrically braced structures; ductility; energy dissipation capacity; load bearing capacity; cyclic load

Ключевые слова: местный предохранитель; концентрически стержневые конструкции; податливость; способность к рассеиванию энергии; грузоподъемность; циклическая нагрузка

Abstract. The concentrically braced system is one of the most common lateral load-bearing systems among the steel structures. This lateral loadbearing system has various apparent forms where the main characteristic of them all is their significant stiffness and lateral strength. The main weakness of the concentrically braced system is buckling in compression. This issue causes that concentric bracings have low compressive load-bearing capacity together with undesirable ductility and limited energy dissipation capacity. In this study to solve this problem use has been made of a heuristic method. In this method a local fuse has been used in the middle of bracing where its periphery and inner circumference have been covered with an auxiliary casing within a casing. The local fuse is designed in a way that after yielding, the bracing undergoes local buckling at this area. But presence of an auxiliary element placed around the fuse prevents this local buckling and thus the bracing would exhibit almost a symmetric behavior during compressive and tensile loadings. Thus the bracing would exhibit a wide and spindle-shaped hysteresis curve under a cyclic loading with desirable ductility and high energy dissipation capacity. Also in this article a numerical study is performed utilizing ABAQUS Ver. 6.12 software to make comparison between concentric bracings with local fuse –auxiliary element (LF-AECB) and usual concentric bracings (UCB) in terms of ductility, energy dissipation capacity and loadbearing capacity. The results of numerical studies have indicated the extraordinary better performance of LF-AECB with respect to that of UCB.

Аннотация. Концентрически стержневая система является одной из наиболее распространенных среди стальных систем с поперечными несущими конструкциями. Эта система имеет различные формы, где основной их характеристикой является значительная жесткость и устойчивость против поперечной силы. Основным недостатком такой системы является изгиб при сжатии. Эта проблема приводит к тому, что концентрические раскосы имеют низкую несущую способность при сжатии вместе с нежелательной податливости и ограниченной способностью к рассеиванию энергии. В этом исследовании для решения проблемы использовался эвристический метод. Местный предохранитель использовался в середине раскоса, где его край и внутренняя окружность были покрыты вспомогательным кожухом внутри корпуса. Местный предохранитель по сжимающей нагрузке спроектирован таким образом, что после прогибания конструкции раскос подвергается местной потери устойчивости. Но наличие вспомогательного элемента, расположенного вокруг предохранителя, предотвращает это, и, таким образом, раскос будет проявлять почти симметричное поведение во время сжимающих и растягивающих нагрузок. Раскос будет иметь широкую и веретонообразную петлю гистерезиса при циклической нагрузке с оптимальной податливостью и высокой способностью рассеивать энергию. Также в этой статье проводится численное исследование с использованием ABAQUS Ver. 6.12 для того, чтобы сравнить концентрический раскос с местным предохранителем-вспомогательным элементом (LF-AECB) и обычными концентрическими раскосами (UCB) с точки зрения податливости, способности рассеивания энергии и несущей способности. Результаты численных исследований показали лучшие эксплуатационные параметры LF-AECB по сравнению с UCB.

Кафя М.А., Качуй А. Поведение концентрических раскосов с встроенным предохранителем по сжимающей нагрузке // Инженерно-строительный журнал. 2018. № 2(78). С. 16–29.

1. Introduction

The concentric braced systems are one of the most applicable systems in steel structures. These systems due to having high stiffness and lateral load bearing with respect to other structural systems have been under focus of attention. The main weakness of these structural systems is buckling of the bracing under compressive loading. Therefore when these structures undergo a cyclic loading, they exhibit an undesirable ductility with low energy dissipation capacity. Hence, researchers from around the world have performed extensive studies to solve this problem in concentric bracings. In continuation, some of these studies are cited.

One of the solutions for enhancing ductility and energy dissipation in concentric braced structures is use of energy dissipation elements located at the intersection of bracings. In this respect application of the rings made of steel tubes as energy dissipater element at intersection with the bracing has been investigated both analytically and experimentally by Abbasnia et al. [1]. The results of these studies have shown that these bracings possess wide and stable hysteresis curves. One of the disadvantages of this system is the certain dimensions of the steel tubes incorporated in the steel rings which cause dimensional restrictions. For this purpose Andalib et al. [2], introduced steel rings made of plates as a replacement for the initial rings and in this respect they have performed an experimental and numerical study to investigate performance of the mentioned rings. The steel rings made of steel plates include two semi rings which are connected to the bracing via some connections and form a single ring. The results of Andalib et al. [2] studies exhibit wide and stable hysteresis curves for the rings made of the steel plates.

The off-center bracing system (OBS) is one of the invented systems to improve the concentric braced structures [3]. In this structural system, the tensile element is not straight and when a lateral load is exerted on the system, its initial geometry changes. Therefore the load-deformation curve of these systems is in the nonlinear geometric form. Moghaddam and Estekanchi [4] in their study on these systems found that the load-deformation diagram of OSBs follows a nonlinear hardening pattern with two yielding points. Then they subjected the single-story and two-story OBS structures to the seismic loading using this pattern. The results of these analyses indicated that the OBS structural system has a behavior similar to that of the Base Isolation system and has a good strength against lateral loads. Bazzaz et al. [5–8] have used a ductile annular steel element to enhance behavior of these systems (OBS-C systems). The results of this study have exhibited higher ductility and greater energy dissipation of this structural system with respect to the OBS system. In another study [9] which has been performed to make comparison between OBS-C systems and diagonal bracing systems with ductile steel rings i.e. DBS-C, the better behavior of OBS-C system in terms of ductility and energy dissipation capacity has been observed.

Use of two-level or multi-level control systems is another method for improving the seismic behavior of structures which has recently been under focus of attention of researchers [10–12]. The main idea in these structural systems, is combination of different control systems with various stiffness and strength values which results into desirable energy absorption in the structure for various earthquake intensities. In one of this study, Zahrai and Vosooq [11] introduced a dual system in which use has been made of the combination of vertical link beam and knee elements to maintain energy absorption. In this structural system, in order to improve the seismic performance, the vertical link beam is used as an energy absorption element in the small loads area and knee elements are used for energy absorption under intense earthquakes. Another system created for implementing the idea of two-level control systems, is the passive tube in tube control system.

Use of ductile fuse elements in the diagonals of concentric braced structures, is another method to improve their seismic behavior. Rezai et al. [13] investigated the effect of different cases of implementing local fuses on the behavior of bracing elements in an experimental study. The result of their study revealed that the fuse elements with appropriate lateral restraints exhibit a stable hysteretic response with high energy absorption and large non-elastic deformation capacity characteristics. In another studies by Legeron et al. [14] and Desjardins et al. [15], they investigated the application of local ductile fuses in the concentric bracings with single-angle section to reduce demand of the acting load on the connection to avoid the need for its strengthening. In this study the tensile capacity of the bracing has been reduced equal to the connection capacity. The Legeron et al. [14] studies showed that implementing ductile local fuses would effectively reduce the seismic load demand acting upon the bracing connections and would prevent their strengthening.

One of the other invented structural systems for improving seismic performance of the structures with concentric bracings is application of the buckling restrained brace (BRB) [16–20]. In this structural system attempt is made that using bracings which include a casing and core, the main shortcoming of the

concentrically braced structural systems which is buckling in compression is removed [16, 17 and 19].The structures with BRBs, present symmetric and stable hysteresis curves which also have significant capacity in terms of ductility and energy dissipation. Furthermore, in the BRB structural system, the non-elastic deformations are entirely and uniformly distributed over the length of buckling restrained bracing and thus damage to other structural elements is prevented.

In this study a novel method is introduced for improving the seismic performance of concentric braced frames. In this method, use has been made of a fuse element in the middle of the bracing (Fig. 1). Design of this element is in a way that after yielding of the bracing at this point, it undergoes local buckling.

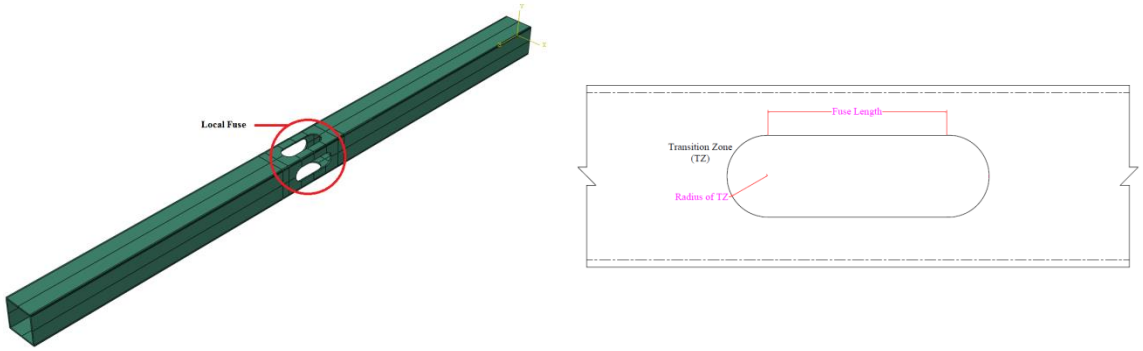

(a) Local fuse position in brace **(b) Details of local fuse**

Figure 1 Local fuse in LF-AECB

To prevent local buckling of the bracing an auxiliary element in the form of casing within casing is used at the fuse area, as shown in Figure 2. This auxiliary element which covers the periphery and inner circumference of the fuse, allows the bracing to resist against local buckling of the fuse and thus prevents loss of the compressive loadbearing. This issue causes that the bracings equipped with fuses and auxiliary elements under cyclic loads to have wide and stable hysteresis curves together with desirable ductility and energy dissipation capacity. Also in this study using ABAQUS Ver. 6.12 [21] a comparison has been made between performances of the concentric bracings with local fuse-auxiliary element (LF-AECB) and usual concentric bracings (UCB), under cyclic pseudo-static loads. In continuation, a complete introduction of LF-AECB bracing and the obtained results from the numerical study will be presented.

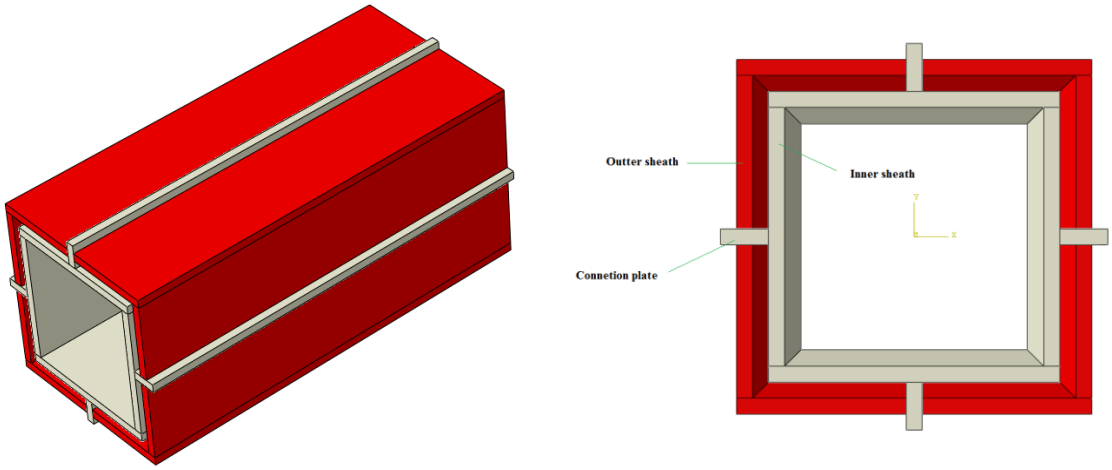

(a) View of auxiliary element **(b) Section of auxiliary element**

Figure 2 Auxiliary element in LF-AECB

2. Methods

2.1. Introduction of LF-AEBC bracing

LF-AEBC bracings are comprised of two parts. The first part is the local fuse implemented at the middle of the bracing area and the second part is the auxiliary element placed at the fuse area to prevent its local buckling. The local fuse used in the bracing, as shown in Fig. 1, is created by reducing the cross section area of the bracing and has a semi-circular transition zone to prevent stress concentration. To calculate the cross section area of the fuse, first the demand exerted load on the bracing (P_u) should be obtained from the analyses. After calculating P_u from Eq. (1), it is concluded:

$$P_u = T_{u,fuse} \tag{1}$$

where, $T_{u,fuse}$is the ultimate tensile loadbearing capacity of the fuse. The value of $T_{u,fuse}$ could be calculated from Eq. (2):

$$T_{u,fuse} = A_{fuse}.F_u \tag{2}$$

In Eq. (2), A_{fuse} and F_u are the fuse cross section area and ultimate stress of the bracing, respectively. Now regarding Eqs. (1) and (2), the fuse cross section area could be calculated from Eq. (3):

$$A_{fuse} \leq \frac{P_u}{F_{u,fuse}} \tag{3}$$

After calculating the fuse cross section area, the required cross section area of the bracing is calculated. For this purpose according to Eq. (4), the fuse ultimate tensile capacity should be taken less than 80 % of the yielding capacity of the bracing:

$$A_{fuse}.\ F_{u,fuse} \leq 0.8.A_g.F_y \tag{4}$$

In the above equation, A_g and F_y are the required cross section area and yielding stress of the bracing materials, respectively. In the above equation, the reason for selecting a coefficient value of 0.8 is to ensure lack of overall yielding of the bracing before the fuse reaches its ultimate capacity, as entire yielding of the bracing causes significant reduced stiffness after its yielding and thus according to Eq. (5), its buckling capacity also decreases proportionally. This issue causes that before the fuse reaches its ultimate loadbearing capacity, the bracing undergoes overall buckling and consequently the expected performance of LF-AEBC bracing system in terms of energy dissipation capacity and expected ductility is not happened.

$$P_{Cr} = \frac{\pi^2.E}{\lambda^2} \tag{5}$$

In the above equation, E is the materials elastic modulus and λ is the slenderness ratio of the element under compression. Regarding Eq. (4), the required cross section area could be calculated using Eq. (6):

$$A\_g \geq (A\_fuse.\ F\_(u,fuse))/(0.8\ .F\_y) \tag{6}$$

It should be mentioned that with respect to Eq. (1), the capacity of the bracing designed according to Eq. (6), is equal to that of the fuse and the loadbearing capacity of the bracing overall cross section area would not affect its loadbearing capacity.

In LF-AEBC bracings, the fuse length is calculated in a way that the fuse buckling occurs after its yielding, so that maximum use of the fuse capacity is utilized for dissipating the input energy to the structure. Respecting this issue, Eq. (7) should be established in LF-AEBC bracings:

$$P_{Cr,fuse} \geq T_{u,fuse} \tag{7}$$

In the above equation, $P_{Cr,fuse}$ is the fuse buckling capacity. The $P_{Cr,fuse}$ value could be calculated from Eq. (8):

$$P_{Cr,fuse} = \frac{\pi^2.E.I_{min,fuse}}{L_{fuse}^2} \tag{8}$$

In the above equation, $I_{min,fuse}$ and L_{fuse} are the minimum moment of inertia and fuse length, respectively. Now respecting Eqs. (2), (7) and (8) the L_{fuse} value could be calculated from Eq. (9):

$$L_{fuse} \leq \sqrt{\frac{\pi^2.E.I_{min,fuse}}{A_{fuse}.\ F_{u,fuse}}} \quad (9)$$

The second component in LF-AEBC bracings is the auxiliary element. The auxiliary elements generally include the external and internal areas of the fuse with 1mm distance from the fuse walls so that they could not affect the fuse loadbearing capacity. The philosophy behind existence of the auxiliary element in LF-AEBC bracing is to prevent local buckling of the bracing in the fuse area. As is evident from Fig. 2, for bracings with box section, this element is comprised of one internal casing with rectangular shape and one external casing with four angle-section elements. These two casings are connected to each other by connecting plates which have passed through the fuse area. The connecting plates' lengths should be exactly equal to the fuse length plus the length of its transition areas to prevent displacement of the auxiliary element over the bracing length. The thickness of connecting plates should also be taken in a way that they do not buckle over the length. Also the length of auxiliary element should be taken at least 15cm greater than the two ends of the fuse transition area.

2.2. Introduction of the numerical models

In this study in order to investigate the effect of implementing local fuse together with auxiliary element on the behavior of concentric bracings, a numerical study utilizing ABAQUS Ver. 6.12 [21] has been conducted. Regarding that all non-elastic deformations in structures equipped with LF-AEBC bracings occur within the fuse area, in this study only the behavior of these bracings under cyclic pseudo-static displacement loads has been investigated, as the behavior of this element under cyclic load would indicate overall behavior of the structure under lateral loads. According to Figure 3, to investigate the behavior of LF-AEBC bracings and making comparison between response of these bracings and that of the concentric bracings, two models of B14 and B20-LF-AE are modeled using Solid Element and with fixed end condition in ABAQUS Ver. 6.12 [21] software. In this paper, model B14 represents the UBC and model B20-LF-AE represents the LF-AECB.

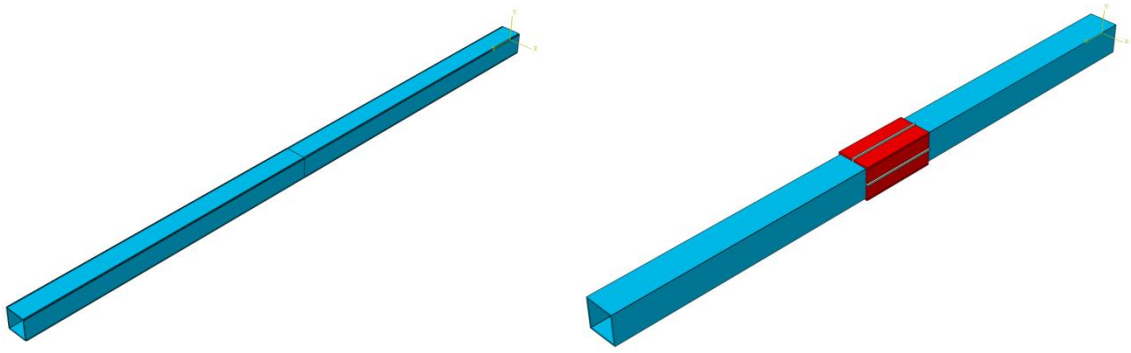

(a) B14 **(b) B20-LF-AE**

Figure 3 Analytical models

The geometric characteristics of structural models are shown in Table 1. Also the materials characteristics utilized in these models are given in Fig. 4 and Table 2. The cross section area of the local fuse implemented in model B20-LF-AE has been obtained based on Eq. (3) and assuming that P_u value is equal to 117 Tons. The local fuse length also is selected 20cm based on Eq. (9). Also transition area of the fuse is a semicircle with a radius of 45.8mm. Regarding the fuse length and the transition area length, the length of auxiliary element is taken equal to 50cm.

Table 1 Geometric characteristics of structural

Models	Brace section	Brace area	Brace length	LF length	LF area	Transition Zone radius	Inner sheath section	Outer sheath section	Connection plate section	Auxiliary element length
B14	Box 14*14*0.6	32.16	400.00	none	none	none	none	none	none	none
B20-LF-AE	Box 20*20*0.8	60.80	400.00	20.00	31.55	4.58	19.8*19.8*1	Four 11.4*11.4*1 angle member	3*1	50.00

Note: The unite of lengths and areas are Cm and Cm²

Кафя М.А., Качуй А. Поведение концентрических раскосов с встроенным предохранителем по сжимающей нагрузке // Инженерно-строительный журнал. 2018. № 2(78). С. 16–29.

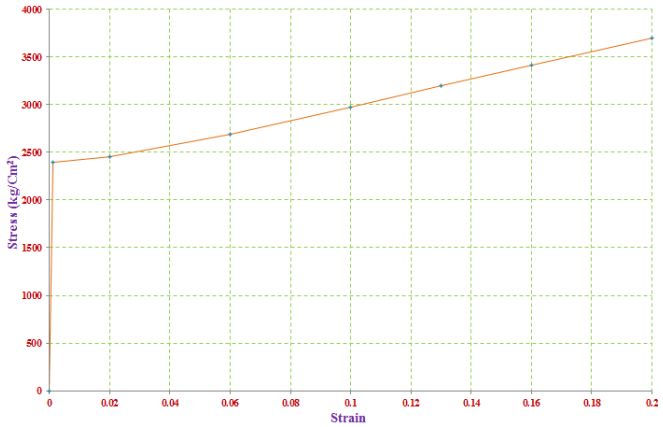

Figure 4 Strain-stress curve of steel material used in the analytical models

Table 2 Material properties used in the analytical models

Element material	Elastic Modulus	Yielding stress	Yielding strain	Final stress	Final strain
ST37	2000000	2400	0.0012	3700	0.20

Note: The unit of stresses is Kg/Cm²

Model B14 is a UCB with equal cross section and tensile capacity equal to those of B20-LF-AE bracing. This model is built to make comparison between seismic behavior of LF-AEBC bracings and that of the UCBs which have equal ultimate tensile capacities. In the next section the responses of the models are compared to each other. Also to perform pseudo static analysis of the structural models and comparing their responses, the ATC-24 loading pattern has been utilized according to Figure 5.

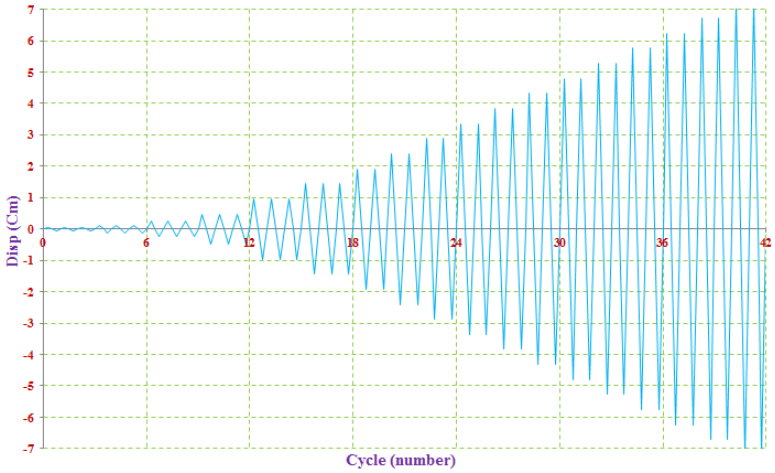

Figure 5 ATC-24 load pattern used in pseudo static analysis

3. Results and Discussion

In this section, the results obtained from analysis of models B14 and B20-LF-AE are investigated. First, the corresponding hysteresis curves of the mentioned models obtained from pseudo-static analyses are accurately investigated. Then, models B14 and B20-LF-AE are compared to each other in terms of ductility, loadbearing capacity and energy dissipation capacity.

3.1. Interpretation of model's hysteresis curves

In this section the interpretation of hysteresis curves has been presented. In Fig. 6 the hysteresis curve of model B14 has been shown. As expected, this model has yielded at 77 tons load and a corresponding displacement of 0.5cm. But contrary to what is expected, this model has buckled in the first cycle of loading after yielding. The reason for premature buckling of the bracing is related to significant reduction in the plastic stiffness of the material with respect to its elastic stiffness. Based on the theoretical calculations, the elastic buckling load of model B14 is 458 tons. Therefore its plastic buckling load would be equal to 1.3 tons, because the plastic stiffness of material is 0.003 its elastic

stiffness. Thus, as during yielding, the available load in the bracing is greater than the plastic buckling load, the bracing has immediately undergone buckling.

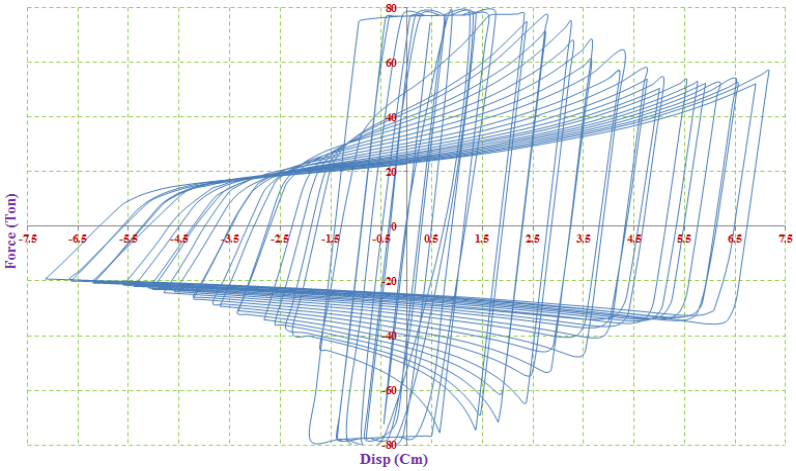

Figure 6 Hysteresis curve of B14

Also after yielding, due to hardening of the steel it was expected that model B14 would enhance its tensile loadbearing capacity with a positive slope in the hysteresis curve, but according to Figure 6, the opposite was observed. The reason for this reduction in tensile loadbearing capacity after yielding of model B14 is also related to the premature buckling of this element. This issue is explained in detail in the next section. Finally model B14 failed at the tensile load of 57 tons and the compressive load of 19 tons and the corresponding ultimate displacement of 7.2 cm in both tension and compression cases. Figure 7 shows the deformed situation of model B14 for its ultimate cyclic loading.

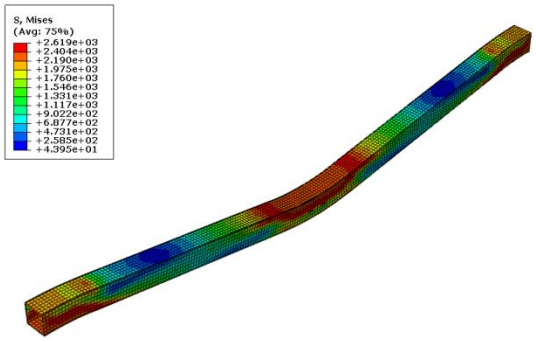

Figure 7 Deformed shape of B14 in final cyclic loading

The hysteresis curve of model B20-LF-AE has been shown in Figure 8. As seen in this figure, the hysteresis curve of this model is wide and spindle shaped which indicates desirable and good performance of this type of bracing in terms of ductility and energy dissipation capacity.

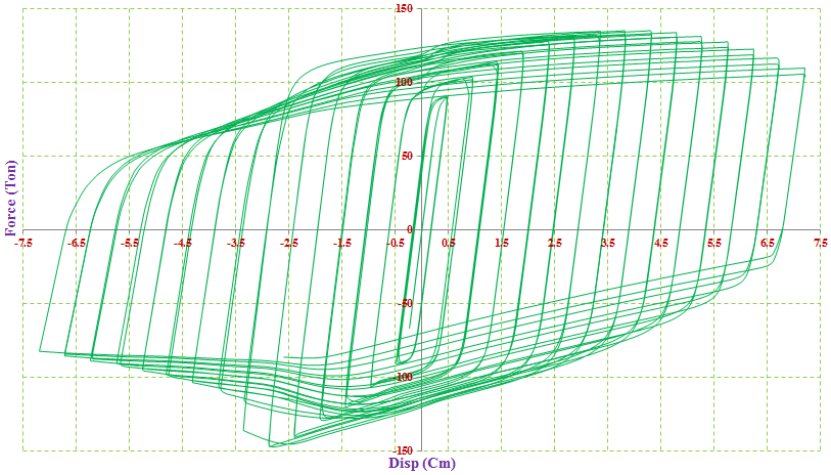

Figure 8 Hysteresis curve of B20-LF-AE

This model has yielded at 76 tons and the corresponding displacement of 0.33 cm. In this model, after yielding and due to significant reduction in the stiffness of the materials, the bracing has undergone buckling. But as was explained before this bracing has been designed in a way that firstly local buckling occurs in the fuse area and secondly, due to presence of the auxiliary element, local buckling of the fuse has been prevented. This is clearly seen in the hysteresis curve of model B20-LF-AE. According to Figure 8, after yielding no loss is seen in the loadbearing capacity of B20-LF-AE bracing and loadbearing capacity of the bracing is increasing both in the compression and tension. But increase in the loadbearing capacity has continued till the bracing has reached overall yielding of the section in the compressive load i.e. a load equal to 146 tons. In this case, as is seen also in Figure 8, the bracing has undergone loss in its compressive loadbearing capacity. The reason for this issue is that when B20-LF-AE bracing has reached its overall yielding capacity, buckling is not as local in the fuse area but in this case overall buckling of the bracing has occurred. Therefore the auxiliary element is no longer able to prevent buckling of the bracing and loss in the compressive loadbearing capacity has occurred. Correspondingly and after overall buckling of B20-LF-AE bracing, its tensile capacity has also degraded. The important issue concerning overall buckling of B20-LF-AE bracing is that loss in the loadbearing capacity in this bracing has occurred with a lower rate with respect to model B14. Finally, B20-LF-AE bracing also has failed in the tensile load of 110 tons and compressive load of 82 tons and a corresponding displacement of 7.2 cm in both compression and tension. Figures. 9 and 10, present the deformation status of B20-LF-AE bracing for the two cases of the final cycle of loading before overall buckling, and the ultimate loading cycle, respectively.

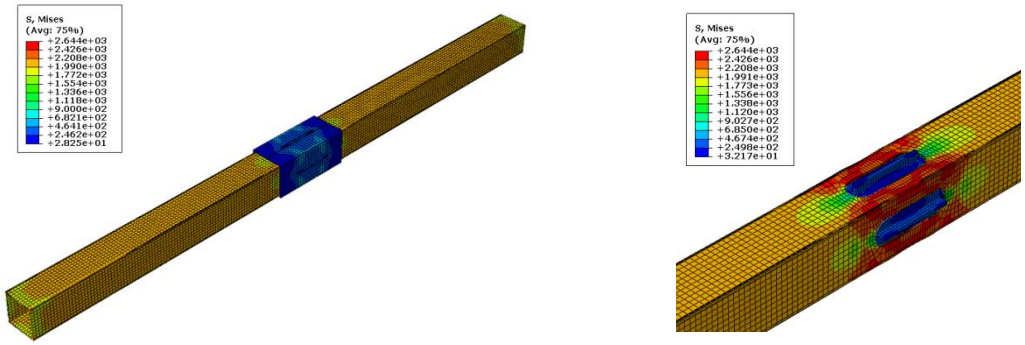

(a) General condition of B20-LF-AE **(b) Condition of local fuse**

Figure 9 Deformed shape of B20-LF-AE in final cyclic loading before buckling

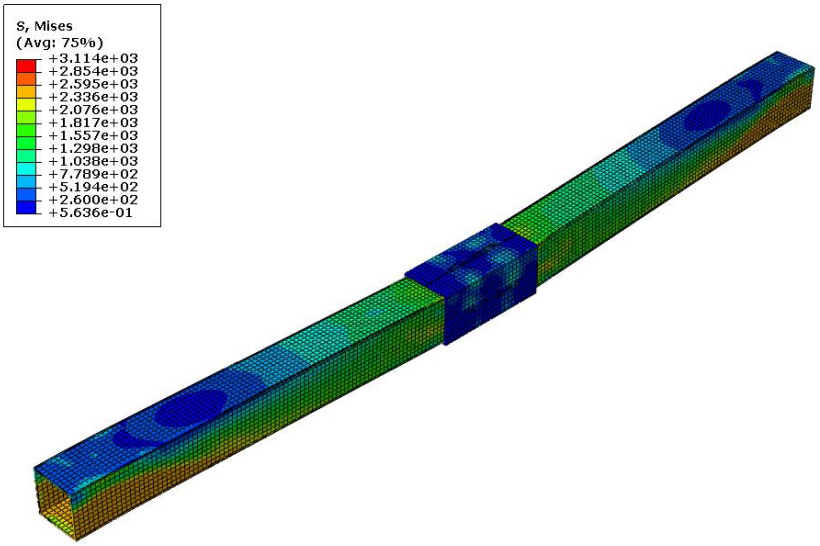

Figure 10 Deformed shape of B20-LF-AE in final cyclic loading

3.2. Comparison between loadbearing capacities of models

To make comparison between loadbearing capacities of models B14 and B20-LF-AE according to Figure 11, the envelope of hysteresis curves corresponding to these two models have been utilized. As is seen in this figure, model B20-LF-AE both in the tensile load and compressive load has far greater loadbearing capacity with respect to that of model B14. In the tension area, as was expected both models

have yielded in their expected tension capacity. But after yielding the behavior of models has been entirely different. The tensile loadbearing capacity of model B14 is reduced after yielding which is not expected. Based on the theoretical calculations, the ultimate tensile loadbearing capacity of this model should have reached 119 tons due to the steel hardening, but because of overall buckling of the bracing and permanent lateral displacement due to it, this model could not achieve its loadbearing capacity.

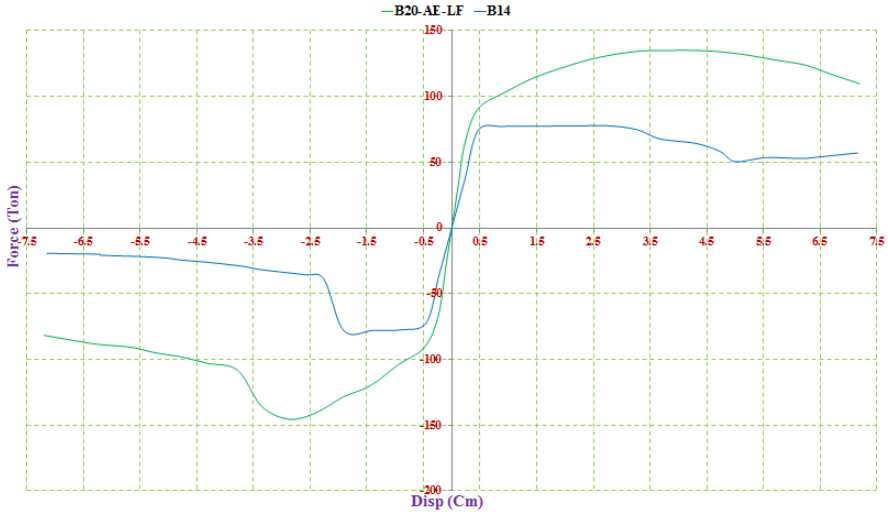

Figure 11 Comparison between envelope curve of analytical models

When the bracing buckles, it experiences lateral displacement. A portion of this lateral displacement remains as residual in the bracing after yielding. This issue causes that the bracing could not become perfectly straight in tension and consequently its tensile loadbearing capacity would reduce. This is clearly seen in Figure 12. This figure shows permanent lateral displacement of the middle point of the bracing with respect to the bracing length (residual relative lateral displacement) for different loading cycles.

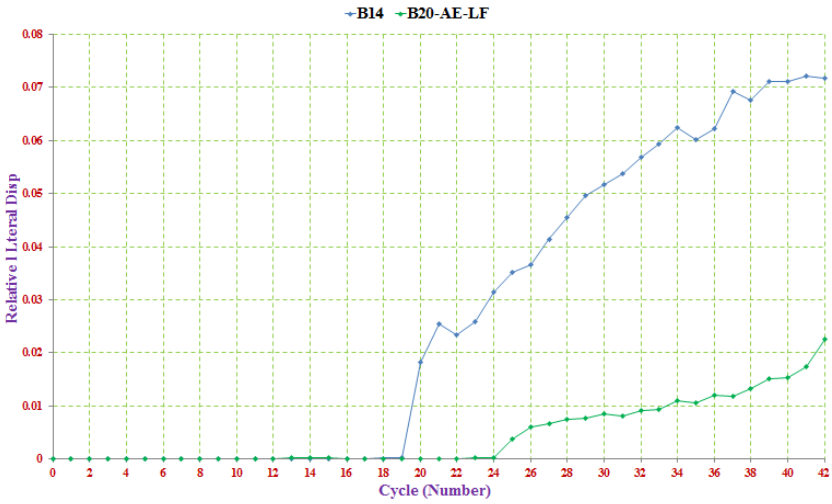

Figure 12 Comparison between residual relative lateral displacement of analytical models

As is seen in Figure 12, the B14 bracing has experienced significant residual lateral displacement from the 20th cycle on. This loading cycle corresponds to an axial displacement equal to 2.4 cm. With respect to the envelope curve of model B14 shown in Figure 11, it is observed that loss in the tensile loadbearing capacity in this model has also started from a displacement value equal to 2.4 cm and with increase in the residual lateral displacement in the next cycles its corresponding tensile force has decreased conversely. Finally, regarding Figure 11, the maximum values of tensile loadbearing capacity and ultimate tensile loadbearing capacity in B14 bracing are 77 tons and 57 tons, respectively. But concerning model B20-LF-AE, the issue is entirely different. The reason is that in this model due to the presence of auxiliary element, the fuse local buckling has been prevented after yielding and thus the bracing not only has not undergone loss in its tensile loadbearing capacity but also its tensile capacity has increased. This increase in the loadbearing capacity has continued up to a load equal to135 tons but after it due to the overall buckling of the bracing, this model has also undergone loss in its tensile

loadbearing capacity. This issue is evident in Figure 12. As is seen in this figure, model B20-LF-AE from cycle 33 on, has experienced a significant residual relative lateral displacement (greater than 0.01 which is equivalent to a lateral displacement greater than 4cm). This cycle corresponds to an axial displacement equal to 5.3 cm, where according to the envelope curve of model B20-LF-AE shown in Figure 11, reduction in the loadbearing capacity of this model has started from this displacement and with increase in the lateral displacement in the next cycles, the corresponding tensile force has decreased, conversely. Albeit it is essential to state that the rate of reduction in the tensile loadbearing capacity in model B20-LF-AE has been considerably less than that of model B14 due to the presence of auxiliary element. This issue is also evident from Figures 11 and 12, so that according to Figure 12, the maximum residual lateral displacement in model B14 was about 29 cm whereas this value in model B20-LF-AE is 69 % less and was equivalent to 9 cm. For model B20-LF-AE also the maximum tensile capacity and ultimate tensile capacity values were 135 tons and 110 tons, respectively. These values were 75 % and 93 % greater than the corresponding values in the model B14, respectively.

As is seen in Figure 11, in the compressive area of model B14, immediately in the first cycle of loading after yielding which corresponds to a load value of 77 tons, has buckled due to reduced Post-elastic stiffness of materials. Regarding Figure 11, the maximum compressive loadbearing capacity and ultimate compressive capacity in model B14 have been 79 tons and 19 tons, respectively. For model B20-LF-AE also after yielding of the fuse, the bracing has undergone local buckling in this area. But due to presence of the auxiliary element, this bucking is prevented and compressive loadbearing capacity of the bracing is increased. Increase in the compressive loadbearing capacity in model B20-LF-AE has continued up to a load value of 146 tons, which corresponds to yielding of the overall section of the bracing in this model. But immediately after this load and due to reduced post-elastic stiffness of the materials, the bracing has undergone overall buckling. Albeit it should be noted that due to presence of the auxiliary element, the rate of reduction in the compressive loadbearing capacity in this bracing is significantly less than that of model B14. This issue could be completely observed comparing envelope curves (Fig. 11) and residual relative lateral displacements of the two models (Fig. 12). Finally and with respect to Figure 11, the maximum and ultimate compressive loadbearing capacities in model B20-LF-AE were 146 tons and 82 tons, respectively. These values were 85 % and 331 % greater than their corresponding values in model B14, respectively. In Table 3, a comparison has been made between the maximum and ultimate tensile and compressive capacity values in models B14 and B20-LF-AE.

Table 3 Loadbearing capacity of models

Models	Max Tension Capacity	Final Tension Capacity	Max Compression Capacity	Final Compression Capacity
B20-AE-LF	135	110	146	82
B14	77	57	79	19
Ratio	1.75	1.93	1.85	4.32

Note: The unite of forces are Ton

3.3. Comparison between ductility in the structural models

In this section comparison has been made between ductility in models B14 and B20-LF-AE. The ductility coefficient values have been obtained separately for the tension and compression areas. In the tension area, the ductility coefficient value, according to Eq. (10), has been calculated by the ratio of the ultimate movement, δ_u^Twhich is equivalent to a corresponding movement equal to 70 % of the maximum force in the bracing in the tensile area to the yielding movement, δ_y.

$$\mu^T = \frac{\delta_u^T}{\delta_y} \tag{10}$$

Based on Figure 11, the $\delta_y$value for models B14 and B20-LF-AE are 0.5 cm and 0.33 cm, respectively. Also the δ_u^T value for both models is 7.2 cm. Thus based on Eq. (10), the tensile ductility coefficient value for models B14 and B20-LF-AE are 14.4 and 21.8, respectively. In other words in the tensile area the ductility coefficient value of model B20-LF-AE has been 1.5 times that of model B14.

In the compression area also the value of ductility coefficient, according to Eq. (11), has been calculated from the ratio of ultimate movement, δ_u^C, which is equivalent to the movement corresponding to a force equal to 70 % of the maximum force of bracing in the compressive area, to the movement corresponding to the first buckling in the model i.e., δ_{FB}.

$$\mu^C = \frac{\delta_u^C}{\delta_{FB}} \tag{11}$$

As two models have undergone buckling immediately after yielding, their δ_{FB} value is equal to their δ_y value. Also according to Figure 11, the δ_u^C values of models B14 and B20-LF-AE are 2.09 cm and 5.25cm, respectively. Then based on Eq. (11), the compressive ductility coefficient value of models B14 and B20-LF-AE are 4.18 and 15.9, respectively. In fact the ductility coefficient of model B20-LF-AE is 3.8 times of that in model B14.

Thus in general and regarding the topics discussed in this section, it is found that LF-AEBC bracings in comparison to the UCBs, exhibit considerably much better ductility. Also in Table 4, the tensile and compressive ductility coefficient values in models B14 and B20-LF-AE have been compared to each other.

Table 4 Ductility of models

Models	Yielding Disp	Final Tension Disp	Tension Ductility Ratio	First Buckling Disp	Final Compression Disp	Compression Ductility Ratio
B20-AE-LF	0.33	7.20	21.82	0.33	5.25	15.91
B14	0.50	7.20	14.40	0.50	2.09	4.18
Ratio	0.66	1.00	1.52	0.66	2.51	3.81

Note: The unite of displacements are Cm

3.4. Comparison between dissipated energy capacities by the structural models

As is in Figures 6 and 8, model B20-LF-AE having a wide and symmetric hysteresis curve, guarantees high energy absorption in this model under lateral loads. Furthermore as is seen in Figures 9 and 10, damage concentration in this model has occurred in the fuse area and this means that in the braced structures with LF-AEBC bracings under lateral loads, the main structural elements are kept safe from damage and inelastic deformations remain in the bracing and are concentrated in the fuse area. To perform a more accurate investigation of the dissipated energy in the numerical models and comparing them to each other, the cumulative dissipated energy (CDE) curves in each loading cycle for models B14 and B20-LF-AE have been shown in Figure 13.

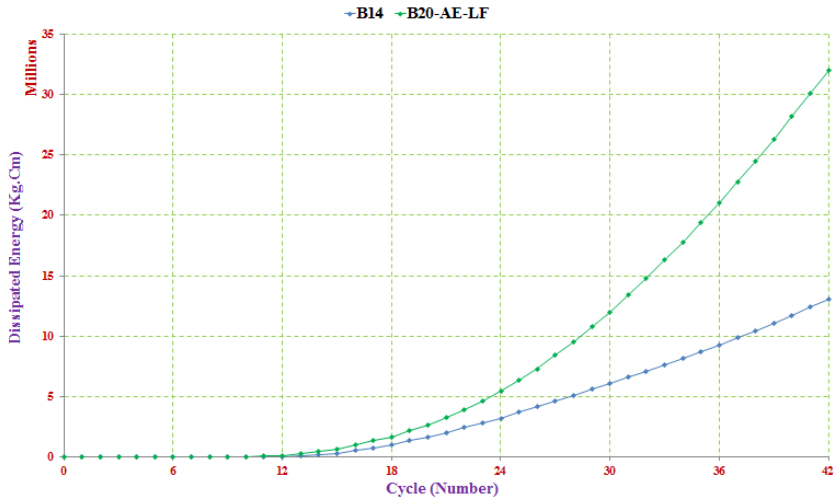

Figure 13 Comparison between cumulative dissipated energy (CDE) of analytical models

As is seen in this figure, the maximum absorbed energy by model B14 was equal to 13047 tons.cm, while this value for model B20-LF-AE was equal to 32016 tons.cm. This means that the amount of overall dissipated energy by bracing B20-LF-AE was 2.45 times of this value for the UCB in model B14. Then regarding that the design loadbearing capacity in both bracings is the same, it is concluded that LF-AEBC bracings have a much better performance in dissipating energy exerted upon the structure with respect to their corresponding UCBs. Also to investigate the effect of overall buckling on the amount of dissipated energy in the bracing, the relative dissipated energy (with respect to the displacement corresponding to each loading cycle) i.e., ECDE/Disp, in each cycle has been shown in Figure 14.

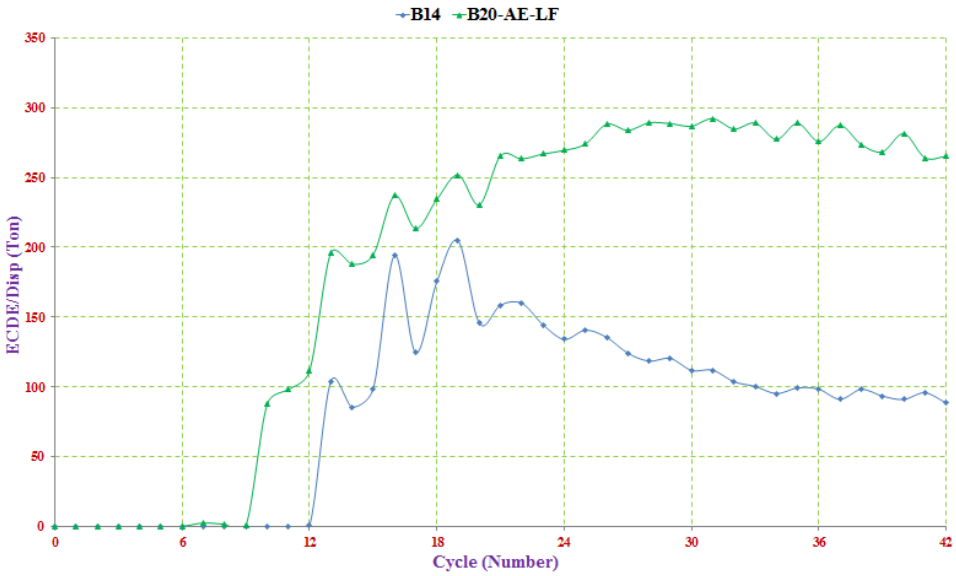

Figure 14 Comparison between ECDE/Disp of analytical models

As is seen in this curve, for model B14 up to cycle 20 of the loading, where no overall buckling has occurred, the curve has an ascending trend which indicates increase in the amount of relative dissipated energy in each loading cycle but immediately after occurrence of buckling of the bracing in the 20th loading cycle, the slope of the curve has turned negative and the amount of relative dissipated energy by model B14 has decreased from this loading cycle on. For model B20-LF-AE also this issue is clearly observed. In this model up to the 33th loading cycle, where overall buckling of the bracing has not occurred, the curve has exhibited an ascending trend which indicates increase in the amount of relative dissipated energy in each loading cycle, but from this loading cycle on where overall buckling has occurred, the slope of the curve also has turned negative and the amount of relative dissipated energy in each cycle has taken a descending trend. The important issue concerning B20-LF-AE bracing is that till overall buckling of the bracing in the cycle 33, the positive slope of the curve is also decreasing. The reason of this is related to the fuse confined capacity. In fact after complete yielding of the fuse and reaching its maximum loadbearing capacity, there is no ascending trend for relative energy absorption and the slope of the curve turns zero and then negative. This case is the best and most ideal possible case for absorbing the input energy to the structure and design of LF-AEBC bracing should be in a way that this kind of energy absorption occurs in the bracing. But in this model, before the slope of the curve turns negative, due to reaching the fuse its maximum capacity, the bracing undergoes overall buckling and this factor has caused negative slope in the curve as shown in Fig. 14 and reduced relative energy absorption by the bracing in each loading cycle. Also comparing the EDCE/Disp curves for models B14 and B20-LF-AE, as shown in Figure 14, it is observed that after overall buckling, the slope of the curve for model B14 decreases with a higher rate in comparison to the slope of the curve corresponding to model B20-LF-AE. This is due to the presence of auxiliary element in model B20-LF-AE and also proves positive performance of this element in the post-buckling behavior of concentric bracings.

4. Conclusion

In this study a complete introduction to the new LF-AEBC bracings has been presented to improve the seismic performance of concentric bracings. In this respect two numerical models of B14 and B20-LF-AE, which represent UCB and LF-AEBC, respectively, have been modeled utilizing ABAQUS Ver. 6.12 [21] and are subjected to the displacement cyclic pseudo-static loading. Then the results of these analyses in terms of loadbearing capacity, ductility and energy dissipation capacity have been compared to each other. In the following the general results obtained from these analyses are presented:

- The hysteresis curve obtained from the analyses results for model B20-LF-AE is a wide spindle-shaped and stable curve. This curve indicates that LF-AEBC bracings could solve the main problem associated with concentric bracings which is buckling and ultimately present a symmetric hysteresis curve.
- Based on the results obtained from this study, the concentric bracings which have an elastic buckling capacity greater than their yielding capacity, immediately after yielding and due to considerable reduced stiffness of their materials, undergo buckling. This issue should be considered in the design of concentric bracings, otherwise design of these structures would be incorrect.

- Generally and based on the obtained results from this study, the LF-AEBC bracings have significantly greater maximum and ultimate tensile and compressive loadbearing capacities in comparison to their corresponding concentric bracings, so that the maximum and ultimate tensile loadbearing capacity of LF-AEBC bracings are about 75 % and 90 % greater than their corresponding UCB bracings, respectively. These values in the compressive area for LF-AEBC bracings are 1.85 and 4.3 times that of their corresponding UCB bracings, respectively.
- Generally and based on the results obtained from this study, the residual lateral displacement due to overall buckling of the bracing causes reduced tensile loadbearing capacity of the bracing and with increase in this displacement, the tensile capacity of the bracing decreases, conversely. It is important to consider this issue that in LF-AEBC bracings with respect to UCB bracings, the rate of reduction in tensile loadbearing capacity is much slower due to presence of the auxiliary element.
- Based on the study results, the tensile and compressive ductility coefficients in LF-AEBS bracings are about 50 % and 280 % greater than their corresponding values in UCB bracings, respectively. This issue indicates the significant impact of implementing LF-AE fuse in concentric bracings to improve ductility in these bracings.
- Based on the results of this study, the amount of dissipated energy by model B20-LF-AE was about 2.5 times of this value for model B14. This issue indicates the much better behavior of LF-AEBS bracings with respect to their corresponding UCB bracings. Also the results of this study showed that in general, the overall buckling of the bracing results into reduced relative dissipated energy in each loading cycle. This reduction occurs with a lower rate for LF-AEBC bracings with respect to UCB bracings, which is due to presence of the auxiliary element and also proves positive performance of this element in the post-buckling behavior of concentric bracings.

References

1. Abbasnia R., Vetr M.G.H., Ahmadi R., Kafi M.A. Experimental and analytical investigation on the steel ring ductility. *Sharif J. Sci. Technol.* 2008. Vol. 52. Pp. 41–48.
2. Andalib Z., Kafi M.A., Kheyroddin A., Bazzaz M. Experimental investigation of the ductility and performance of steel rings constructed from plates. J.*Construct. Steel Res.* 2014. Vol. 103. Pp. 77–88.
3. Moghaddam H., Estekanchi H. On the characteristics of off-centre bracing system. *J.Construct. Steel Res.* 1995. Vol. 35(3). Pp. 361–376.
4. Moghaddam H., Estekanchi H. Seismic behavior of off-centre bracing systems. *J.Construct. Steel Res.* 1999. Vol. 51(2). Pp. 177–196.
5. Bazzaz M., Kheyroddin A., Kafi M.A., Andalib Z. Evaluating the performance of steel ring in special bracing frame. *6th International Conference of Seismology and Earthquake Engineering.* Tehran, Iran. May, 2011.
6. Bazzaz M., Kheyroddin A., Kafi M.A., Andalib Z. Evaluation of the seismic performance of off-centre bracing system with ductile element in steel frames. *Steel Compos. Struct., Int. J.* 2012. Vol. 12(5). Pp. 445–-464.
7. Bazzaz M., Kheyroddin A., Kafi M.A., Andalib Z., Esmaeili H. Evaluating the seismic performance of off-centre bracing system with circular element in optimum place. *Int. J. Steel Struct.* 2014. Vol. 14(2). Pp. 293–304.
8. Bazzaz M., Andalib Z., Kafi M.A., Kheyroddin A. Evaluating the performance of OBS-C-O in steel frames under monotonic load. *Earthq. Struct., Int. J.* 2015. Vol. 8(3). Pp. 697–710.
9. Bazzaz M., Andalib Z., Kheyroddin A., Kafi M.A. Numerical comparison of the seismic performance of steel rings in off-centre bracing system steel rings in off-centre bracing system. *Steel Compos. Struct., Int. J.* 2015. Vol. 19(4). Pp. 917–937.
10. Balendra T., Yu C.H., Lee F.L. An economical structural system for wind and earthquake loads. *J. Eng.Struct*. 2001. Vol. 23. Pp. 491–501.
11. Zahrai S.M., Vosooq A.K. Study of an innovative two-stage control system: Chevron knee bracing & shear panel in series connection. *J. Struct Eng.* 2013. Vol. 47(6). Pp. 881–898.

Литература

1. Abbasnia R., Vetr M.G.H., Ahmadi R., Kafi M.A. Experimental and analytical investigation on the steel ring ductility // Sharif J. Sci. Technol. 2008. Vol. 52. Pp. 41–48.
2. Andalib Z., Kafi M.A., Kheyroddin A., Bazzaz M. Experimental investigation of the ductility and performance of steel rings constructed from plates // J.Construct. Steel Res. 2014. Vol. 103. Pp. 77–88. DOI: 10.1016/j.jcsr.2014.07.016
3. Moghaddam H., Estekanchi H. On the characteristics of off-centre bracing system // J.Construct. Steel Res. 1995. Vol. 35(3). Pp. 361–376.
4. Moghaddam H., Estekanchi H. Seismic behavior of off-centre bracing systems // J.Construct. Steel Res. 1999. Vol. 51(2). Pp. 177–196.
5. Bazzaz M., Kheyroddin A., Kafi M.A., Andalib Z. Evaluating the performance of steel ring in special bracing frame // 6th International Conference of Seismology and Earthquake Engineering. Tehran, Iran. May, 2011.
6. Bazzaz M., Kheyroddin A., Kafi M.A., Andalib Z. Evaluation of the seismic performance of off-centre bracing system with ductile element in steel frames // Steel Compos. Struct., Int. J. 2012. Vol. 12(5). Pp. 445–-464.
7. Bazzaz M., Kheyroddin A., Kafi M.A., Andalib Z., Esmaeili H. Evaluating the seismic performance of off-centre bracing system with circular element in optimum place // Int. J. Steel Struct. 2014. Vol. 14(2). Pp. 293–304.
8. Bazzaz M., Andalib Z., Kafi M.A., Kheyroddin A. Evaluating the performance of OBS-C-O in steel frames under monotonic load // Earthq. Struct., Int. J. 2015. Vol. 8(3). Pp. 697–710.
9. Bazzaz M., Andalib Z., Kheyroddin A., Kafi M.A. Numerical comparison of the seismic performance of steel rings in off-centre bracing system steel rings in off-centre bracing system // Steel Compos. Struct., Int. J. 2015. Vol. 19(4). Pp. 917–937.
10. Balendra T., Yu C.H., Lee F.L. An economical structural system for wind and earthquake loads // J. Eng.Struct. 2001. Vol. 23. Pp. 491–501.
11. Zahrai S.M., Vosooq A.K. Study of an innovative two-stage control system: Chevron knee bracing & shear panel in series connection // J. Struct Eng. 2013. Vol. 47(6). Pp. 881–898.

Кафя М.А., Качуй А. Поведение концентрических раскосов с встроенным предохранителем по сжимающей нагрузке // Инженерно-строительный журнал. 2018. № 2(78). С. 16–29.

12. Cheraghi A., Zahrai S.M. Innovative multi-level control with concentric pipes along brace to reduce seismic response of steel frames. *J.Construct. Steel Res.* 2016. Vol. 127. Pp. 120–135.
13. Rezai M., Prion H., Tremblay R., Bouatay N., Timler P. Seismic performance of brace fuse elements for concentrically steel braced frames. *3rd Proc. of STESSA Conference.* Montréal, Canada, 2000.
14. Legeron F., Desjardins E., Ahmed E. Fuse performance on bracing of concentrically steel braced frames under cyclic loading. *J.Construct. Steel Res.* 2014. Vol. 95. Pp. 242–255.
15. Desjardins E., Legeron F., Ahmed E. Performances of ductile fuses in reducing seismic demand on connections of concentrically steel braced frames. *15th World conference on Earthquake Engineering.* Lisbon, Portugal, 2012.
16. Iwata M., Kato T., Wada A. Buckling-restrained braces as hysteretic dampers. *3rd International Conference STESSA.* Montreal, Canada, 2000.
17. Sabelli R., Mahin S., Chang C. Seismic demands on steel braced frame buildings with buckling-restrained braces. *J. Eng Struct.* 2003. Vol. 25(5). Pp. 655–666.
18. Kiggins S., Uang C.M. Reducing residual drift of buckling-restrained braced frames as a dual system. *J. Eng. Struct.* 2006. Vol. 28(11). Pp. 1525–1532.
19. Hoveidae N., Tremblay R., Rafezy B., Davaran A. Numerical investigation of seismic behavior of short-core all-steel buckling restrained braces. *J.Construct. Steel Res.* 2015. Vol. 114. Pp. 89–99.
20. Maurya A., Eatherton M.R., Matsui R., Florig S.H. Experimental investigation of miniature buckling restrained braces for use as structural fuses. *J.Construct. Steel Res.* 2016. Vol. 127. Pp. 54–65.
21. ABAQUS Ver .6.12. User's Manual, RI, USA, 2012.

12. Cheraghi A., Zahrai S.M. Innovative multi-level control with concentric pipes along brace to reduce seismic response of steel frames // J.Construct. Steel Res. 2016. Vol. 127. Pp. 120–135.
13. Rezai M., Prion H., Tremblay R., Bouatay N., Timler P. Seismic performance of brace fuse elements for concentrically steel braced frames // 3rd Proc. of STESSA Conference. Montréal, Canada, 2000.
14. Legeron F., Desjardins E., Ahmed E. Fuse performance on bracing of concentrically steel braced frames under cyclic loading // J.Construct. Steel Res. 2014. Vol. 95. Pp. 242–255.
15. Desjardins E., Legeron F., Ahmed E. Performances of ductile fuses in reducing seismic demand on connections of concentrically steel braced frames // 15th World conference on Earthquake Engineering. Lisbon, Portugal, 2012.
16. Iwata M., Kato T., Wada A. Buckling-restrained braces as hysteretic dampers // 3rd International Conference STESSA, Montreal, Canada, 2000.
17. Sabelli R., Mahin S., Chang C. Seismic demands on steel braced frame buildings with buckling-restrained braces // J. Eng Struct. 2003. Vol. 25(5). Pp. 655–666.
18. Kiggins S., Uang C.M. Reducing residual drift of buckling-restrained braced frames as a dual system // J. Eng. Struct. 2006. Vol. 28(11). Pp. 1525–1532.
19. Hoveidae N., Tremblay R., Rafezy B., Davaran A. Numerical investigation of seismic behavior of short-core all-steel buckling restrained braces // J.Construct. Steel Res. 2015. Vol. 114. Pp. 89–99.
20. Maurya A., Eatherton M.R., Matsui R., Florig S.H. Experimental investigation of miniature buckling restrained braces for use as structural fuses // J.Construct. Steel Res. 2016. Vol. 127. Pp. 54–65.
21. ABAQUS Ver .6.12. User's Manual, RI, USA, 2012.

Mohammad Ali Kafi,
00982331533755; mkafi@semnan.ac.ir

Ali Kachooee,
00989127910346; ali.kachooee@semnan.ac.ir

Мохаммад Али Кафя,
00982331533755; эл. почта: mkafi@semnan.ac.ir

Али Качуй,
00989127910346;
эл. почта: ali.kachooee@semnan.ac.ir

© Kafi M.A.,Kachooee A., 2018

Kafi M.A., Kachooee A. The behavior of concentric brace with bounded fuse. *Magazine of Civil Engineering*. 2018. No. 2. Pp. 16–29. doi: 10.18720/MCE.78.2.